Chapter 4

Mechanistic Study of Cyclohex-2-enol to Cyclohex-2-enone by High Valent Iron Species: C-H/O-H Bond Activation

4.1 Introduction

The main challenge in synthetic organic chemistry is chemo selective oxidation of C-H bond by natural complexes under mild conditions.[1-5] Heme and non-heme metal complexes with several oxidants such as dioxygen, hydrogen peroxide, m-chloroperbenzoic acid etc. are involved in catalytic oxidation of aliphatic and aromatic C-H bond.[6-8] Ubiquitous dioxygen (O_2) is an ideal oxidant and environmentally benign because water could be obtained as a by-product after reduction, and the redox potential provided by it is more than sufficient to carry out several chemical transformations.[9-14] Normally, the catalytic oxidation of alkenes by dioxygen is not selective, many metal-catalyzed methods have been developed for catalytic oxidation reactions.[15-22] Catalytic properties of iron with dioxygen and its derivatives such as hydrogen peroxide and superoxide are very useful due to the low toxicity of iron in biochemistry.[23] Last several decades, heme and non-heme iron-oxo species have been synthesized and characterized for biomimetic studies.[24-26] High valent Fe^{IV}=O is playing a very important role in the scientific community due to its catalytic properties such as C-H/O-H/N-H activation and oxygen atom transfer reactions of aliphatic and aromatic compounds.[8,27-30] Fe^{IV}=O species have been characterized by X-ray and spectroscopic techniques, and also observed during catalytic reactions with enzymes having iron.[31-43] Role of axial and equatorial ligands can affect the reactivity of iron(IV) during catalytic reactions.[29,38] Most popular example is cytochrome P450, which catalyzes many reactions such as oxidation, reduction, isomerisation and dehydration.[44-45] High valent iron(IV)-oxo containing TMC (1,4,8,11-tetramethyl1,4,8,11-tetraazacyclotetradecane), TPA (tris (2pyridylmethyl)amine), BPMEN (N,N'-dimethyl-N,N'-bis(2-pyridylmethyl)ethane-1,2-diamine) and N_4Py (N,N-bis(2-pyridyl methyl)bis(2-pyridyl)methylamine) are also involved in epoxidation and hydroxylation of aliphatic and aromatic compounds.[6,46]

Apart from Fe^{IV}=O, Fe^{V}=O species is also a very reactive intermediate in many catalytic transformation reactions.[6,46,47] Iron complexes by reacting with oxygen form high valent metal complexes without any electron or proton transfer.[48] But, the reaction of a metal complex with oxygen is rare without any reductant.[49-59] Fe(V) species is reported in several oxidation reactions involving hydrogen and organic peroxide.[60] Fe(V)-oxo species has also been shown as an active intermediate in the Rieske dioxygenase enzyme family.[61-77] The species with TMC, TPA, BPMEN etc. have been reported spectroscopically and their high-resolution crystal is also observed.[31,78-80] Many spectroscopic techniques such as electronic, magnetic circular dichroism, Raman, electron paramagnetic resonance (EPR) and M*ö*ssbauer spectroscopy, are commonly used to characterize the Fe(V)-oxo complexes.[28,30,79-80,81] Synthetic functional models of Fe(V)-oxo complex carry out many C-H and C=C oxidation reactions.[66,82] Fe(V)-oxo with tetra-amido complexes are also reported and well-characterized spectroscopically and shows selective hydroxylation towards aliphatic compounds but has a limited theoretical study on catalytic activity by the complex.[63,83] Allylic oxidation is of great interest because of the easy availability of olefins and the allylic transformation gives either allylic alcohol or α,β-unsaturated carbonyl compounds and these are attractive synthetic targets.[84-90] General methodology creates several issues such as regioselectivity, stereo selectivity, poor compatibility and over oxidation during allylic oxidation.[91-96] The C-H bond activation in preference to the C=C bond is observed by mononuclear non-heme M^{IV}=O (M = Fe and Ru with ligands $RuClCp(PTA)_2$ and $[RuCp(PTA)_2(H_2O\text{-}\kappa O)]OTf$) complexes (where Cp = cyclopentadiene and PTA = 1,3,5-triaza-7-phosphaadamantane).[97-98] Such C-H bond activation depends upon the allylic C-H bond dissociation energies (BDE) of the olefin substrates.[99-103] Iron-oxo complexes are greener, popular and powerful oxidants and these are used for allylic oxidations giving rise to valuable intermediates for the pharmaceutical industry. The cyclohex-2-enone is an important intermediate used in organic synthesis,

medicinal chemistry, pesticide chemistry, materials science, rubber industry etc.[104] Cyclohexene is a good raw material for industry, which can be accessed cheaply by selective hydrogenation of benzene.[105-106] In cyclohexene, two oxidation sites are present, one for hydrogen abstraction of an allylic C-H bond and the other for oxygen-atom transfer to the C=C bond give many products such as *trans/cis*- cyclohexane- 1,2- diol, adipic acid, cyclohex-2-enol or cyclohex-2- enone. Cyclohex-2-enone is useful in organic synthesis, medicinal chemistry, pesticide chemistry, materials science etc.[101-102,107-108] To synthesize cyclohex-2-enone from cyclohex-2-enol is very important and has wide applications in pharmaceutical and synthetic organic industries.[97-98] A very little theoretical study has been done on the O-H bond activation of the cyclohex- 2- enol. A computational investigation of active catalyst species plays an important role in O-H and C-H bond activation to get better insights into electronic structures and mechanistic study of catalytic transformation reactions. Here, we have reported a mechanistic study of selective allylic oxidation of cyclohex-2-enol by Fe(V)-oxo with tetra-amido ligand and electronic structures/energetic of intermediates involves during the catalytic cycle followed by origin of higher reactivity between O-H and C-H activation.

4.2 Computational Details

Gaussian09 suite of programs is used for all calculations.[109] Method assessment on the transition metal complexes had been carried out using several functionals such as B3LYP[110-111], B3LYP-D2[112], wB97XD,[113] B97D,[112] TPSSh,[114] OLYP,[115] MP2,[116] M06,[117] and M06-2X[118-120] in previous studies.[6-8] Among all tested functionals, B3LYP, B3LYP-D2 and wB97XD were predicted correct spin states of the transition metal complexes.[6-8] The functional B3LYP-D2 includes dispersion correction which was found as superior.[6,46,121] So here, we have employed B3LYP-D2 functional for all the calculations. B3LYP-D2 functional

is used for all geometry optimizations and the mechanism of metal-mediated catalytic reactions[7,122-133] is understood by state-of-the-art functional. Although we have also done calculations with other functionals such as B3LYP and wB97XD for further confirming barrier height during the reaction (see Table AX 4.1 - AX 4.6 of appendix). The LACVP basis set comprising the LanL2DZ-Los Alamos effective core potential for the transition metal (Fe)[134-136] and a 6-31G[137] basis set for the other atoms (C, H, N and O) have been employed for geometry optimization, and the optimized geometries are then used to perform single-point energy calculations using a TZVP[29,138-139] basis set on all atoms. PCM solvation model is used for computing the solvation energies using acetonitrile as a solvent. The quoted DFT energies are B3LYP-D2 solvation at TZVP basis set incorporating free-energy corrections at LACVP basis set at a temperature of 298.15 K. The transitions states were characterized by a single imaginary frequency which pertains to the desired motion as visualized in Chemcraft[140] and also by intrinsic reaction coordinate calculations. To confirm the minima on the potential-energy surface (PES) and to obtain zero-point energy corrections frequency calculations are done on the optimized structure at the B3LYP-D2 level. The fragment approach available in Gaussian09 is employed to aid smooth convergence in cases of radical intermediates. Common notation of $^{mult}A_{pathway}$ is used throughout, the mult superscript denotes the total multiplicity of the species, A denotes transition/intermediate/product and the pathway subscript denotes the possible pathways.

4.3 Results and Discussion

Based on experimental studies, electronic structures and bonding aspects of high valent iron species are discussed followed by the mechanism of allylic oxidation along with the oxygen attack of cyclohex-2-enol using tetra-amido iron(V)-oxo species. Two possible mechanistic pathways are proposed based on the O-H (***pathway a***) and C-H (***pathway b***) bond activation

of the cyclohex-2-enol to form cyclohex-2-enone which are discussed separately followed by a comparative study.

4.3.1 Mechanistic study of cyclohex-2-enol to cyclohex-2-enone

After a detailed study on the electronic structure of $[(TAML)Fe^{V}(O)]^{-}$ species in chapter 3, we have a keen interest to do a mechanistic study towards the O-H and C-H bond activation of cyclohex-2-enol using $[(TAML)Fe^{V}(O)]^{-}$ species. A significant spin density on the ferryl oxygen can be witnessed for the O-H/C-H bond activation of the cyclohex-2-enol. Based on previous mechanistic studies,[6-8,27-30] here we have proposed a mechanistic study for the conversion of cyclohex-2-enol to cyclohex-2-enone by the putative Fe^{V}=O species. Here we have proposed two possible pathways (***pathway a:*** O-H and ***pathway b:*** C-H bond activation) by which the reaction can take place for the formation of the final product, cyclohex-2-enone. In ***pathway a***, hydrogen abstraction of the O1-H1 of the cyclohexen-2-enol by ferryl oxygen can proceed via ts_a-1 (see Scheme 4.1) for the generation of radical at the oxygen of cyclohex-2-enol followed by abstraction of the second hydrogen (C1-H2) via ts_a-2 leading to the final product (see Scheme 4.1), while in ***Pathway b***, the abstraction of hydrogen from the carbon atom (C1-H2) can occur via ts_b-1 (see Scheme 4.1) where OH is attached by the ferryl oxygen followed by abstraction of the hydrogen (O2-H1) of the same carbon atom via ts_b-2, leading to the final product (see Scheme 4.1). The mechanism of ***pathway a*** and ***b*** is discussed separately.

4.3.1.1 ***Pathway a*****:** In this pathway, at first, the abstraction of hydrogen of O1-H1 by Fe(V)-oxo takes place via the formation of the transition state ($^{4,2}ts_a$-1; see Scheme 1).[29,141-142] Our DFT calculations show that the barrier height for the abstraction of hydrogen on the low spin surface is computed to be at 64.9 kJ/mol and this is the ground state compared to the high

spin surface ($^{4}ts_{a}$-1) at 71.5 kJ/mol (see Figure 4.1). The low spin as the ground state is also calculated by functionals B3LYP and wB97XD (see Figure AX 4.1 of appendix).

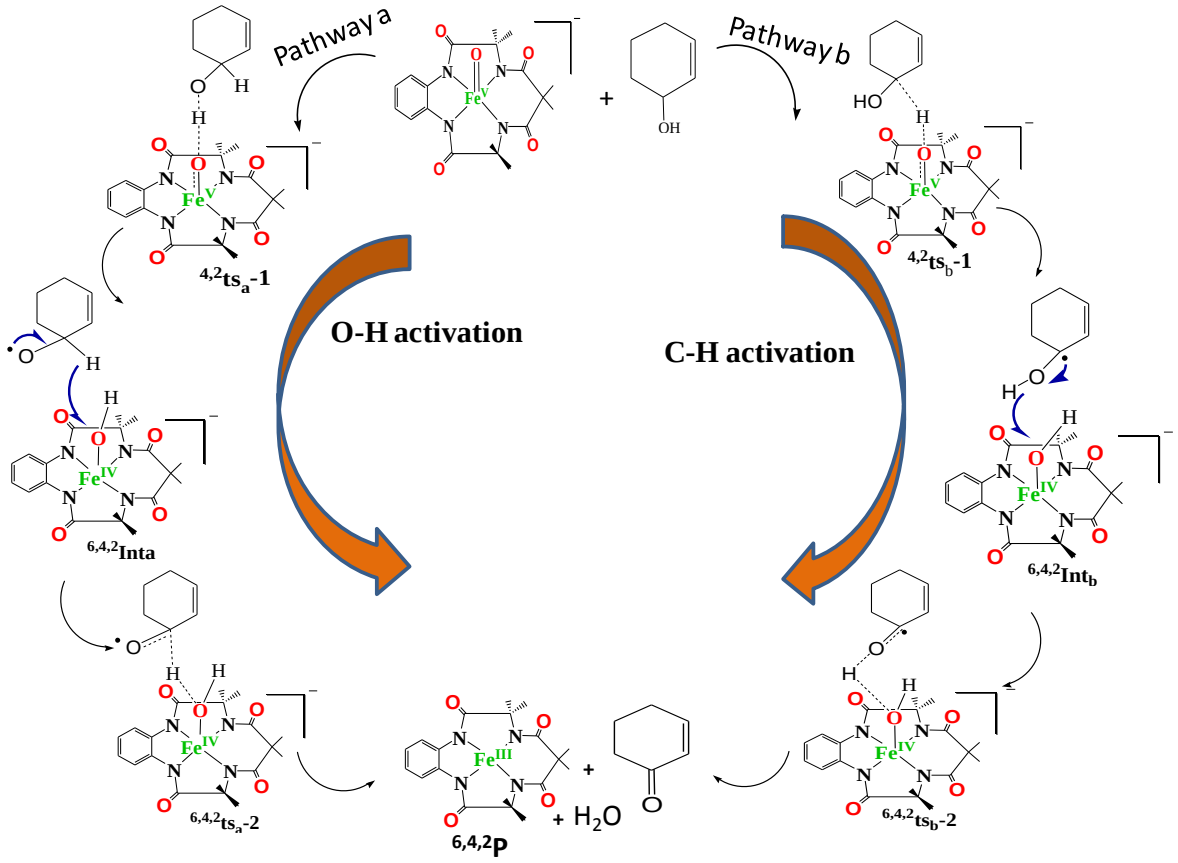

Scheme 4.1. Adapted DFT mechanism for the formation of cyclohex-2-enone from cyclohex-2-enol by Fe^{V}=O species.

The lower computed energy surfaces suggest that the O-H bond activation can show two-state reactivity, and this is also found with the functional B3LYP. The computed energy profile with these functional suggests that the dispersion plays a significant effect on reducing the energy barrier of the transition state which is ca. 20 kJ/mol lower in energy. This shows an interesting impact upon the addition of the dispersion (see Figure AX 4.1 and AX 4.2 of appendix). Imaginary frequency and intrinsic reaction coordinate (IRC) calculations confirm the formation of the transition state.

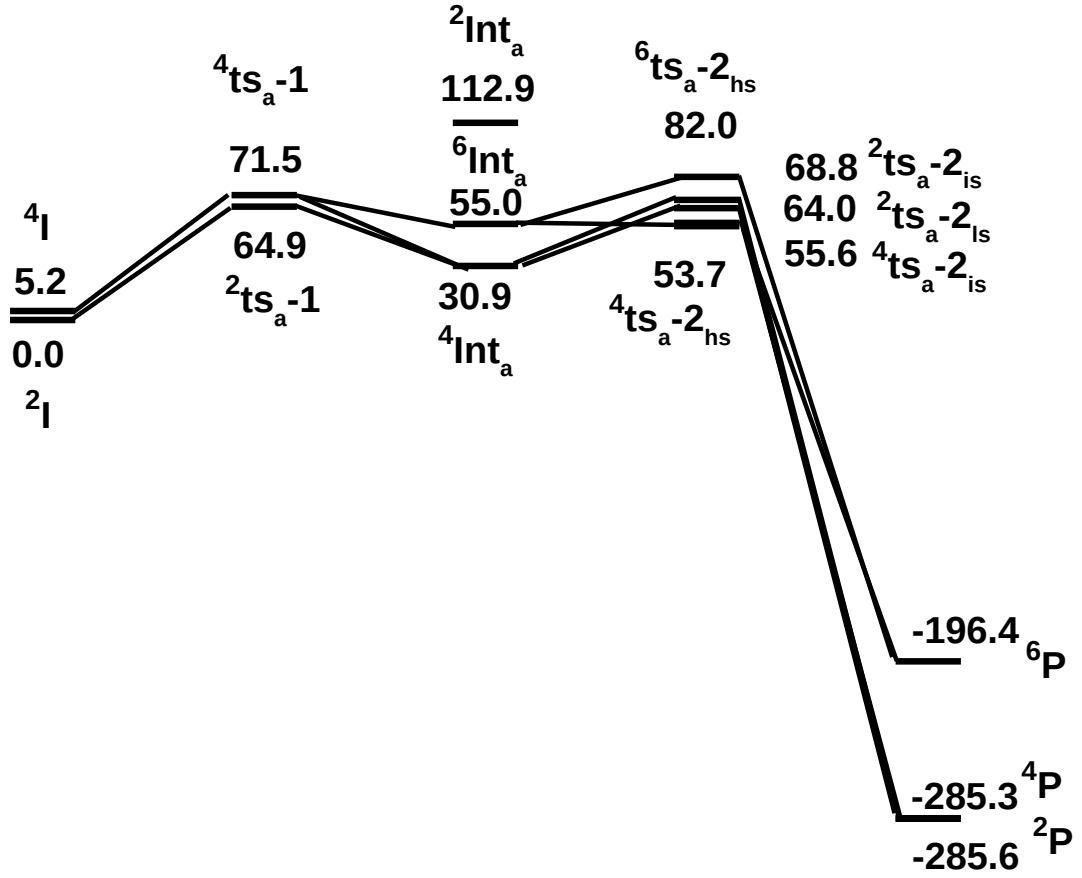

Figure 4.1. B3LYP-D2 computed energy surface for the formation of cyclohex-2-enone from cyclohex-2-enol via O-H bond activation by Fe^{V}=O species (ΔG in kJmol^{-1}).

The computed Fe−O bond in the ^{2}ts$_a$-1 elongates to 1.737 Å compared to its corresponding bond lengths in the Fe(V)=O from 1.630 Å, the O1-H1 bond length comes closer to 1.077 Å, H1-O2 elongates from 0.979 to 1.397 Å and C1-O2 shortens from 1.476 to 1.435 Å (see Table 4.1 and Table 4.2). The DFT optimized structure of the transition state (^{2}ts$_a$-1) and its corresponding spin density plot with B3LYP-D2 functional are shown in Figure 4.2. These computed structural parameters of the ^{2}ts$_a$-1 confirm the formation of the transition state for the abstraction of hydrogen from the cyclohex-2-enol by the ferryl oxo oxidant as shown in Figure 4.2. These parameters of the transition states show that the ^{2}ts$_a$-1 looks more towards the next step (Int$_a$) compared to the ^{2}ts$_a$-1 and this unfolds the reason for the lowest barrier at the low spin surface (see Table 4.1).

Table 4.1. B3LYP-D2 computed structural parameters of the $[Fe^{V}(TAML)O]^{-}$ species, intermediates transition states and product of *Pathway a*.

	Bond lengths (Å)										Bond angle (°)					
	Fe-N1	Fe-N2	Fe-N3	Fe-N4	Fe-O1	O1-H1	O1-H2	H1-O2	H2-C1	C1-O2	Fe-O1-H1	Fe-O1-H2	O1-H1-O2	O1-H2-C1	N1-Fe-N3	N2-Fe-N4
^{4}I	1.914	1.914	1.878	1.878	1.664	-	-	-	-	-	-	-	-	-	155.7	155.8
^{2}I	1.898	1.898	1.887	1.886 1.87[1]	1.630 1.58[1]	-	-	-	-	-	-	-	-	-	152.2	152.1
$^{4}ts_{a}$-1	1.892	1.882	1.871	1.875	1.752	1.067	-	1.387		1.423	119.0		169.6		153.8	156.9
$^{2}ts_{a}$-1	1.894	1.897	1.874	1.872	1.737	1.077	-	1.397		1.435	109.0		169.7		156.9	152.0
^{6}Int	1.911	1.919	1.889	1.905	1.906	154.7	-	-	-	-	-	-	-	-	154.7	150.3
^{4}Int	1.877	1.877	1.879	1.879	1.803	0.982	-	-	-	-	-	-	-	-	155.0	155.0
^{2} Int	1.932	1.834	1.910	1.830	1.760	161.5	-	-	-	-	-	-	-	-	161.5	143.6
$^{6}ts_{a\text{-}hs}$	1.884	1.912	1.875	1.877	2.010	-	1.297		1.327	-	-	115.9	-	173.8	160.4	153.1
$^{4}ts_{a\text{-}hs}$	1.901	1.904	1.887	1.881	1.974	-	1.470		1.226	-	-	129.7	-	170.7	155.6	155.9
$^{4}ts_{a}$-2_{is}	1.887	1.898	1.883	1.890	1.886	-	1.598		1.174	-	-	130.5	-	166.7	156.2	153.9
$^{2}ts_{a}$-2_{is}	1.903	1.911	1.883	1.889	1.956	-	1.276		1.335	-	-	132.8	-	174.9	156.9	155.1
$^{2}ts_{a}$-2_{ls}	1.877	1.878	1.880	1.870	1.848	-	1.457		1.224	-	-	131.8	-	173.3	160.2	155.7
^{6}P	1.984	1.984	1.924	1.924	-	-	-	-	-	-	-	-	-	-	159.7	159.7
^{4}P	1.864	1.867	1.868	1.864	-	-	-	-	-	-	-	-	-	-	171.9	171.9
^{2}P	1.851	1.872	1.853	1.865	-	-	-	-	-	-	-	-	-	-	170.9	171.2

Table 4.2. B3LYP-D2 computed spin density values of the $[Fe^{V}(TAML)O]^{-}$ species, intermediates, transition states and product of *Pathway a*.

	Fe1	O1	H1	H2	O2	C1
^{4}I	1.279	0.757	-	-	-	-
^{2}I	1.061	0.585	-	-	-	-
$^{4}ts_{a}$-1	1.607	0.290	-0.017	-	0.519	-
$^{2}ts_{a}$-1	1.690	0.139	0.012	-	-0.447	-
^{6}Int	3.202	0.381	0.005	-	-	-
^{4}Int	1.788	0.036	0.010	-	-	-
^{2}Int	0	0	0	-	-	-
$^{6}ts_{a}$-2_{hs}	3.173	0.216	-	0.109	0.557	0.141
$^{4}ts_{a}$-2_{hs}	3.143	0.201	-	-0.119	-0.698	0.010
$^{4}ts_{a}$-2_{is}	2.319	0.038	-	0.110	0.795	-0.031
$^{2}ts_{a}$-2_{is}	2.468	0.051	-	-0.108	-0.625	-0.095
$^{2}ts_{a}$-2_{ls}	0.513	0.026	-	0.120	0.717	-0.016
^{6}P	3.914	-	-	-	-	-
^{4}P	2.663	-	-	-	-	-
^{2}P	1.187	-	-	-	-	-

Although all the three functionals show similar architecture the plot of the transition state ($^{4}ts_{a}$-2) (see Figure AX 4.1 of appendix) but the computed structural parameters are in the good agreement with B3LYP-D2 compared to B3LYP and wB97XD suggesting that dispersion drives transition state much nearer to the next step. The bond angle of Fe-O1-H1 is 109.0˚ suggests that electron transfer can take place by π-pathway (see Scheme 4.2) and this is also confirmed by the eigenvalue plot (see Figure 4.3 and Figure 4.4).[6,27] In the transition state $^{2}ts_{a}$-1, one of the C-H bond electrons is found to be transferred to $(d_{xz,})^{1}$ orbital (vide infra) and here we have also observed that the energy gap between the (d_{yz}) and (d_{xz}) orbitals increase slightly. Spin density plots (see Figure 4.2a') show that there is a significant increment of electron density at the iron center of the transition state which means an extra electron is coming to the metal center (see Figure 4.3) by π-mechanism (see Scheme 4.2).

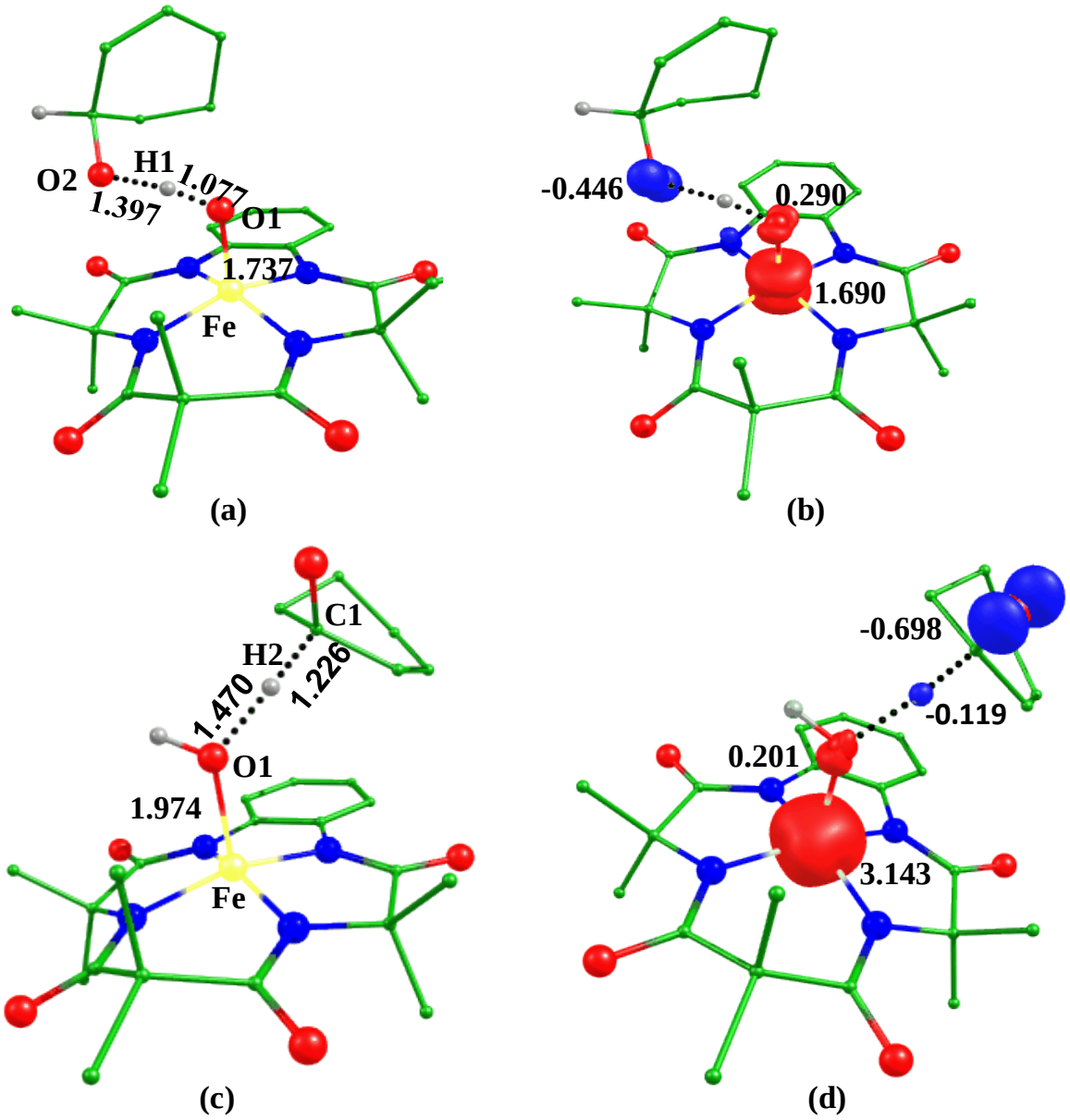

Figure 4.2. B3LYP-D2 a) optimized structure (bond length in Å) and b) its spin density plot of the transition state, $^{2}ts_{a}$-1 c) optimized structure (bond length in Å) and d) its spin density.

This suggests that hydrogen abstraction proceeds by the proton-coupled electron transfer mechanism.[8,28,144] The spin density plot and optimized structure of the ground state are shown in Figure 4.2a,b. The transition state shows that a significant spin density also found on the oxygen of the cyclohex-2-enol indicates radical character generation on it along with carbon center.

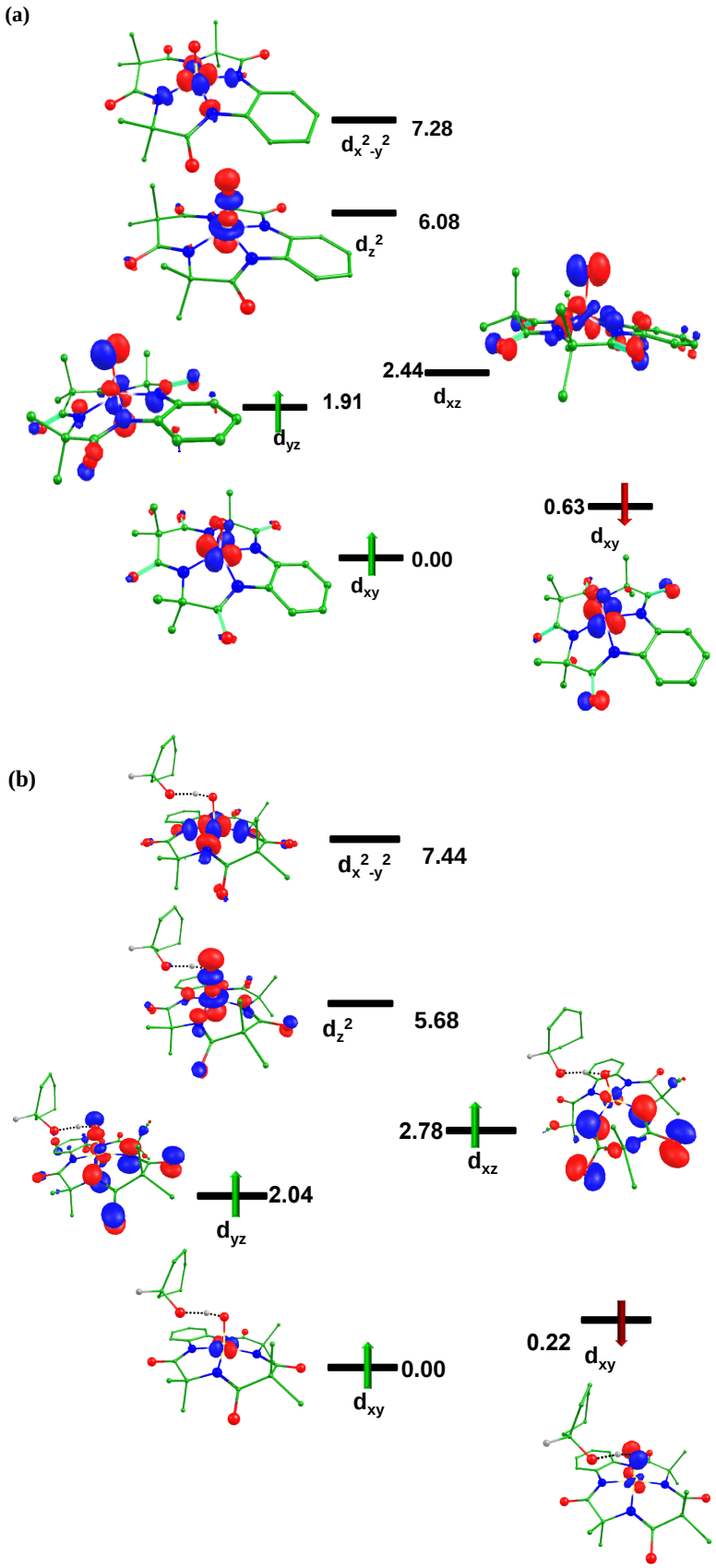

Figure 4.3. Computed Eigen-value plot incorporating energies computed for *d*-based orbitals for alpha and beta spin corresponding to the ground state (^2ts_a-1) (energies are given in eV).

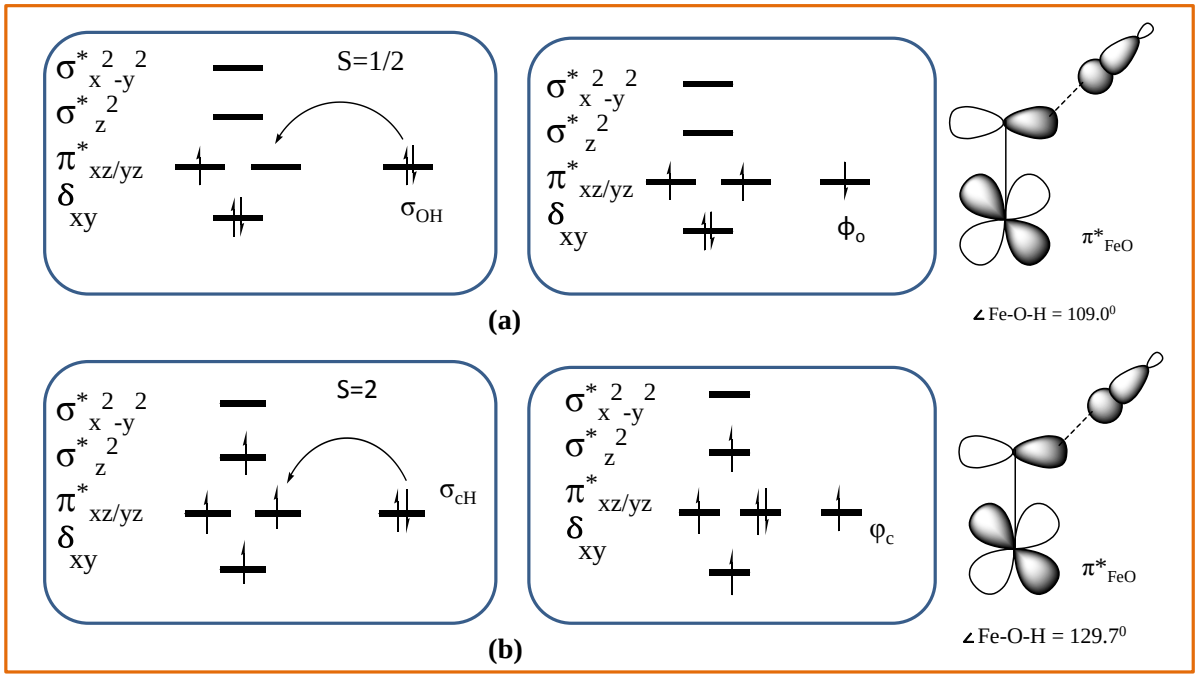

Scheme 4.2. Orbital occupancy diagrams for the H-abstraction of (a) $^{2}ts_{a}$-1 and (b) $^{4}ts_{a}$-2_{hs}.

The absolute variation in the magnitude of spin densities are found to be larger in the B3LYP-D2 compared to B3LYP (see Table 4.3 and Table AX 4.4 of appendix) revealing that dispersion drives the transition state much closer to the next step. After the first hydrogen abstraction, the intermediate Int_a is formed which has three possible spin states ($^{6,4,2}Int_a$). Our results show that the $^{4}Int_a$ is found to be the ground state with 24.1 and 82.0 kJ/mol, respectively, for $^{6}Int_a$ and $^{2}Int_a$ states are higher in energy (see Figure 4.1). The results are also almost inconsistent with functional B3LYP and wB97XD (see Table AX 4.1 and AX 4.2) and the ground state is also observed in previous studies with other architectures.[6,144] In the next step, the abstraction of the second hydrogen which is directly attached to carbon (C1) of cyclohex-2-enoxide radical (see Scheme 4.1) to form transition state ts_a-2. The barrier height for the hydrogen abstraction is found to be 53.6 kJ/mol on the $^{4}ts_{a}$-2 transition state with other spin surfaces that are higher in energy (see Figure 4.1 and 4.2c,d). The Fe-O1, O1-H2 and H2-C1 bond lengths are computed to be 1.974 Å, 0.980 Å and 1.226 Å. Computed

structural parameters with the other two functionals are also shown in Table AX 4.1 and Table AX 4.2 of appendix. After this, leads to the formation of final product cyclohexen-2-one. The energetic reveals the doublet spin state is the most stable for product and the overall thermodynamic stabilization of -285.6 kJ/mol (see Figure 4.1). A significantly large thermodynamic stability of the final product can be abled for C-H/O-H bond activation for forthcoming catalytic cycles.

4.3.2.2 ***Pathway b:*** Similar to ***Pathway a***, Fe(V)-oxo abstracts hydrogen (H2) which is directly attached to the carbon from cyclohex-2-enol to form a transition state ($^{4,2}ts_b$-1).[6-8,27-30,83,103,145,146] The barrier height for the hydrogen abstraction for high and low spin surfaces is found to be 84.5 and 60.7 kJ/mol, respectively (see Figure 4.4).

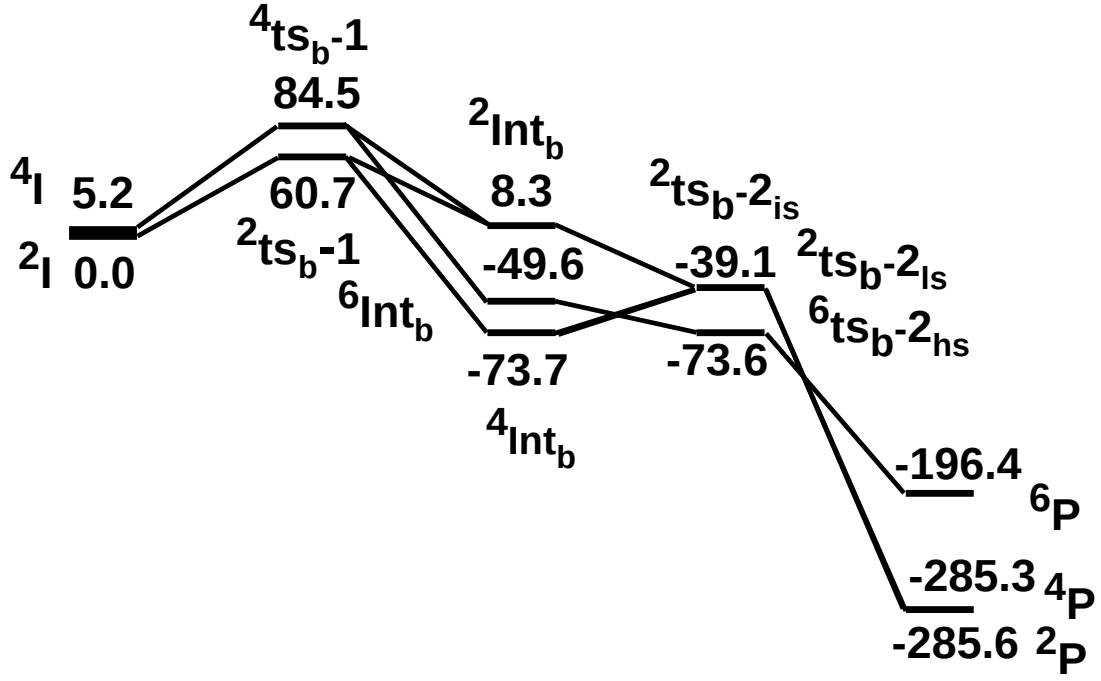

Figure 4.4. B3LYP-D2 computed energy surface for the formation of cyclohex-2-enone from cyclohex-2-enol via C-H bond activation by Fe^{V}=O species (ΔG in $kJmol^{-1}$).

The low spin state ($^{2}ts_b$-1) is found to be the ground state and this barrier is comparatively lower than the C-H bond activation of cyclic aliphatic compounds by other iron(IV)-oxo

species.[8,26] The optimized structure and spin density plot of the ground state is shown in Figure 4.5a,b. Our computed structural parameters show that the Fe-O bond in $^{2}ts_{a}$-1 elongates to 1.740 Å from 1.630 Å, and the O1-H2 bond length is 1.470 Å and the H2-C1 is 1.178 Å in the $^{2}ts_{b}$-1.

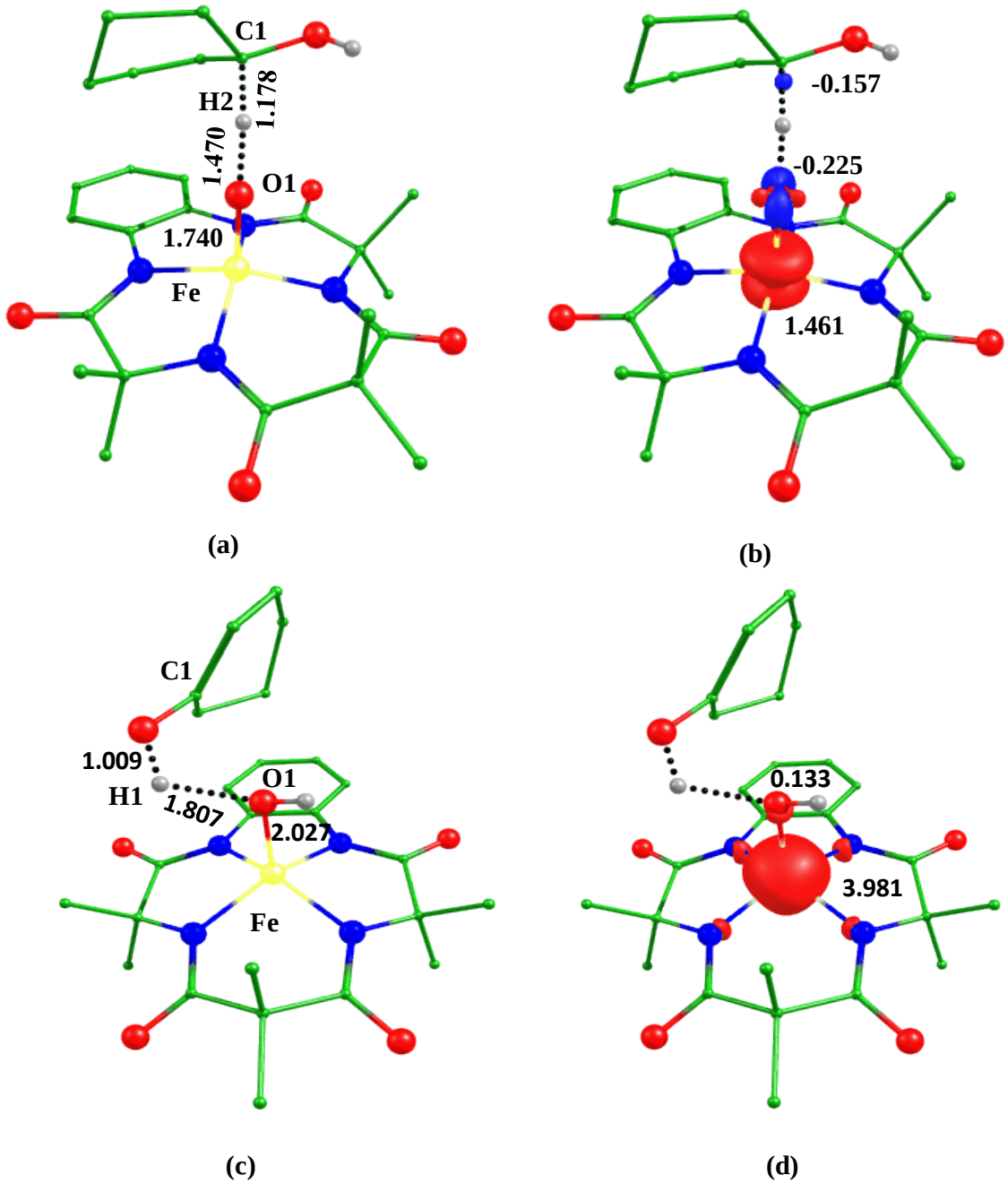

Figure 4.5. B3LYP-D2 a) optimized structure (bond length in Å), b) its spin density plot of the transition state $^{6}ts_{b}$-2_{hs}, c) optimized structure (bond length in Å) and d) its spin density plot of the transition state $^{6}ts_{b}$-2_{hs}.

These parameters confirm the formation of the transition state. The formation of the transition state is also confirmed by the IRC calculation. The bond angle between Fe-O1-H2 is 116.0˚. This shows that the hydrogen abstraction takes place by π-pathway (see Table AX 4.5 of appendix). There is a significant increment in spin density ($\Delta\rho$ = 0.460; see Table AX 4.6 of appendix) indicates that an extra electron is coming to d_{xz} orbital which is also be seen in the eigenvalue plot (see Figure 4.3(a) and 4.6). From all these observations, we can see that the hydrogen abstraction takes place along with electron transfer and this is known as proton-coupled electron transfer which is similar to the $^{2}ts_{a}$-1.[8,28,143] After the hydrogen abstraction, an intermediate is formed ($^{6,4,2}Int_{b}$). The $^{4}Int_{b}$ is computed to be the ground state and the other surfaces $^{6}Int_{b}$ and $^{2}Int_{b}$ are found at 24.0 kJ/mol and 65.3 kJ/mol higher in energy. In the next step, ferryl hydroxide abstracts the hydrogen from the hydroxyl group of cyclohexenolyl radical to form transition states (ts_{b}-2) with five possible spin states due to the interaction of metal electrons with an unpaired electron on the allyl carbon atom, but unfortunately, we are not able to get three transitions due to convergence issues.

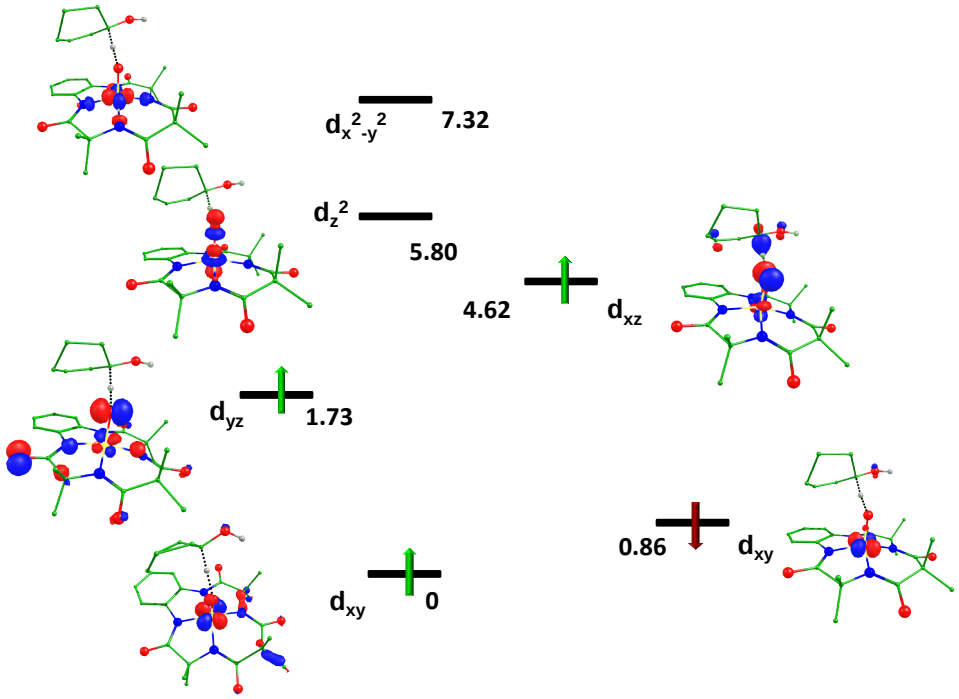

Figure 4.6. Computed Eigen-value plot incorporating energies computed for d-based orbitals for alpha and beta spin corresponding to the ground state ($^{2}ts_{b}$-1) (energies are given in eV).

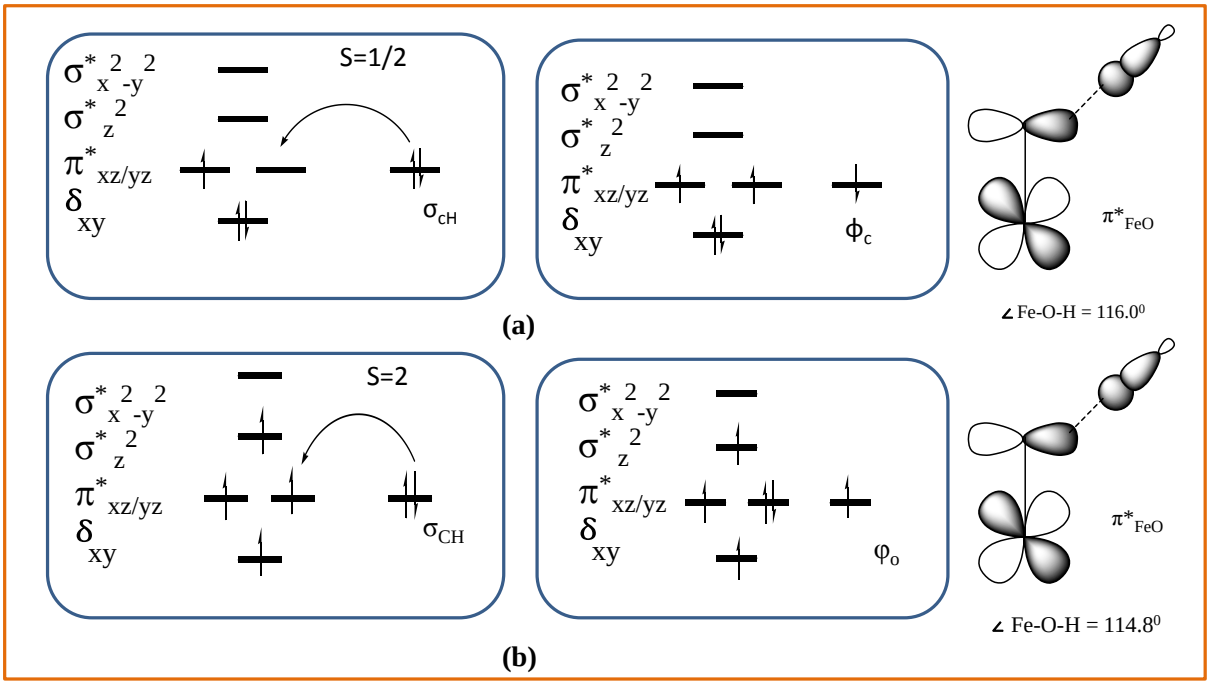

Scheme 4.3. Orbital occupancy diagrams for the H-abstraction of (a) $^{2}ts_{b}$-1, and (b) $^{6}ts_{b}$-2_{hs}.

Although this is a barrier-less transition state (see Figure 4.4). However, we are able to get transition state on four possible spin surfaces of the ts_{b}-2 with the functional B3LYP (see Table AX 4.5 and 4.6 of appendix) and these computed results also support the barrier-less transition (also see Figure 4.4). The spin density plot and optimized structure of the ground state of the transition ts_{b}-2 are shown in Figure 4.5c,d. After this, it is converted into the product which is stabilized by -285.6 kJ/mol on the doublet surface and the overall thermodynamic stabilization is already discussed in ***pathway a***.

4.3.2 Epoxidation of cyclohex-2-enol

Apart from the C-H/O-H bond activation, we have further elucidated the epoxidation on the C=C bond of cyclohex-2-enol by the Fe^{V}=O oxidant. For this, we have also optimized the transition state of oxygen attack on cyclohex-2-enol and our DFT calculations show that the barrier height of this transition is computed to be 78.3 kJ/mol on the low spin surface (^{2}ts)

with a high spin surface lies at (^{4}ts) at 88.4 kJ/mol (see Figure 4.7). The optimized structure and spin density plot of the ground state (^{2}ts) are shown in Figure 4.8a,b. The Fe-O1 bond length elongates to 1.683 Å from 1.630 Å and the C1-O1 bond length is 1.940 Å confirm the formation of the transition state of oxygen attack. A significant spin density (ρ = 0.483) on C2 shows the formation of radical at the carbon atom. This leads to the formation of intermediate (Int) lie at 45.8 kJ/mol (^{6}Int), 19.9 kJ/mol (^{4}Int), and 53.9 kJ/mol (^{2}Int). Second transition state lie at 16.4 kJ/mol (^{4}ts-2$_{hs}$), 43.2 kJ/mol (^{2}ts-2$_{hs}$) and 59.1 kJ/mol (^{6}ts-2$_{hs}$) (see Figure 4.7).

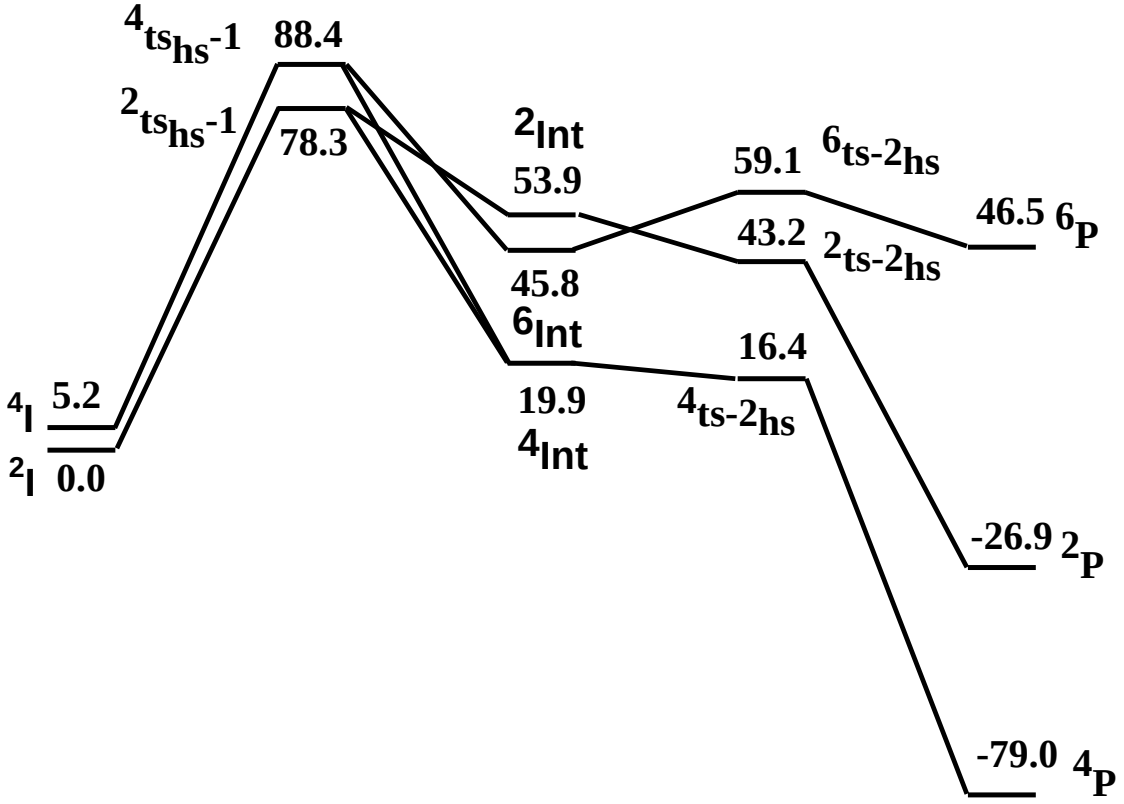

Figure 4.7. B3LYP-D2 computed energy surface for the formation of cyclohexane epoxide from cyclohex-2-enol via O atom transfer by Fe^{V}=O species (ΔG in $kJmol^{-1}$).

This barrier shows that the first step is the rate-determining step. During the second transition state, the C2-O1 bond distance is 2.204 Å. The optimized structure and spin density plot of ^{4}ts-2$_{hs}$ is shown in Figure 4.8c,d. The second transition state leads to the formation of the

epoxide. The barrier height of the oxygen attack is significantly larger as compared to C-H and O-H bond activation of cyclohex-2-enol, so we can safely ignore the epoxidation pathway here.

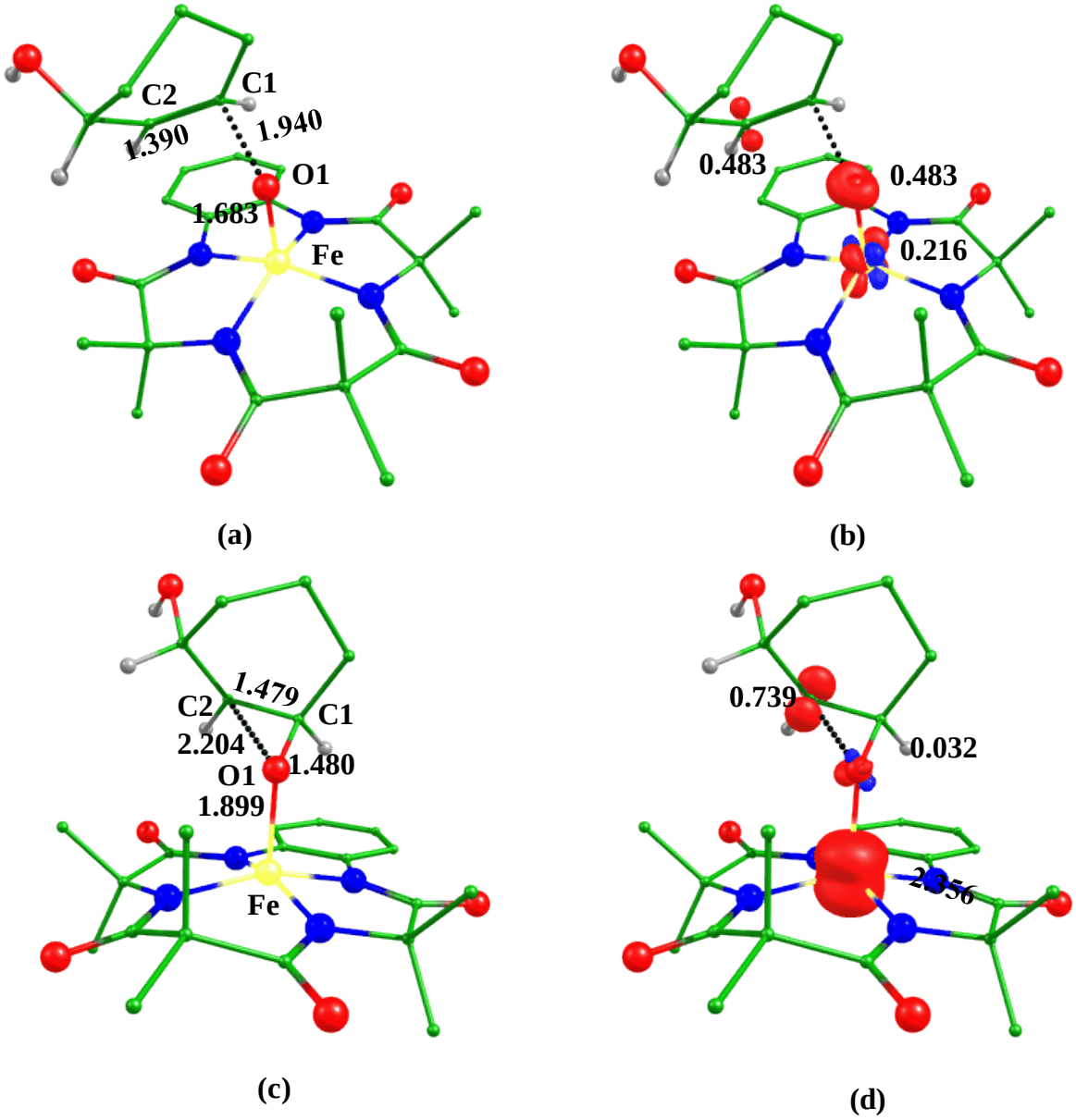

Figure 4.8. B3LYP-D2 a) optimized structure (bond length in Å) of low spin surface (^{2}ts) and b) its spin density plot.

4.3.3 Comparative study of O-H *vs.* C-H bond activation

Dual catalytic abilities are observed for the TAML iron-oxo complex, where it is found to activate inert O-H/C-H bonds of cyclohex-2-enol.[83,103] The O-H/C-H bond activation

proceeds via doublet spin surface of the Fe(V)=O center. The computed barrier height for the O-H bond activation is relatively larger than that of the C-H bond activation (64.7 *vs.* 60.9 kJ/mol; see Figure 4.9) and this step is the rate-determining step. The Fe-O1 bond length is found in the $^{2}ts_{a}$-1 is 1.737 Å whereas 1.684 Å in the $^{2}ts_{b}$-1 suggested that the Fe-O bond is more shortened in the $^{2}ts_{b}$-1 i.e. transition state looks like more towards the further step (Int_{b}). This unfolds the relatively lower barrier height of the Fe^{V}=O oxidant towards the C-H bond activation rather than the O-H activation. We have also observed that if the bond angle of the ground state of the transition states is nearer to 120° suggests smoothly entering an extra electron into metal *d*-orbital and this can control energy barrier height (see Scheme 4.2 and Scheme 4.3). Both the HOMO of the transition states $^{2}ts_{a}$-1 and $^{2}ts_{b}$-1 clearly show involvement of the π_{OH} and π_{CH} bond activation but larger orbital contribution in C-H bond can reduce barrier height (see Figure 4.10). A significant electron density acquired at the oxygen ($^{2}ts_{a}$-1) and carbon ($^{2}ts_{b}$-1) centers show that the reaction takes place via radical mechanism rather than cationic or anionic. The iron center of the transition $^{2}ts_{a}$-1 gains more electrons compared to the $^{2}ts_{b}$-1 ($\Delta\rho$ = 0.229) indicates proton-coupled electron transfer can take place relatively faster in the O-H bond activation. The energy required for the abstraction of the second hydrogen in the $^{4}ts_{a}$-2 is 53.7 kJ/mol and in the $^{6}ts_{b}$-2 is -73.6 kJ/mol. The activation energy for the second hydrogen abstraction in the ***pathway a*** required 22.8 kJ/mol and it is computed barrier less transition in the ***pathway b*** although the first step in both the pathways is the rate-determining step. Computed structural parameters show that the Fe-O bond elongation during the ts-2 is more in ***pathway b*** than the ***pathway a*** suggested that the $^{4}ts_{b}$-2 is more likely towards the product. The spin density at the iron center in the $^{4}ts_{a}$-2_{hs} is 3.143 and in the $^{6}ts_{b}$-2_{hs} is 3.981. We have observed that the spin density on the iron center has decreased by 0.032 in the case of O-H whereas it has increased by 0.779 in C-H activation during the second transition. The increased spin density at the metal center

indicates that the reaction can take place via the electron transfer which is also confirmed by the eigenvalue plot. Electron and proton transfer takes place simultaneously in both the pathways O-H and C-H bond activation and this indicates the process of formation of cyclohex-2-enone from cyclohex-2-enol proceeds via proton-coupled electron transfer (PCET) mechanism.[28,143] From our DFT calculations, the second transition state in the C-H bond activation is found as the barrier-less step.[6,27,46,147-148]

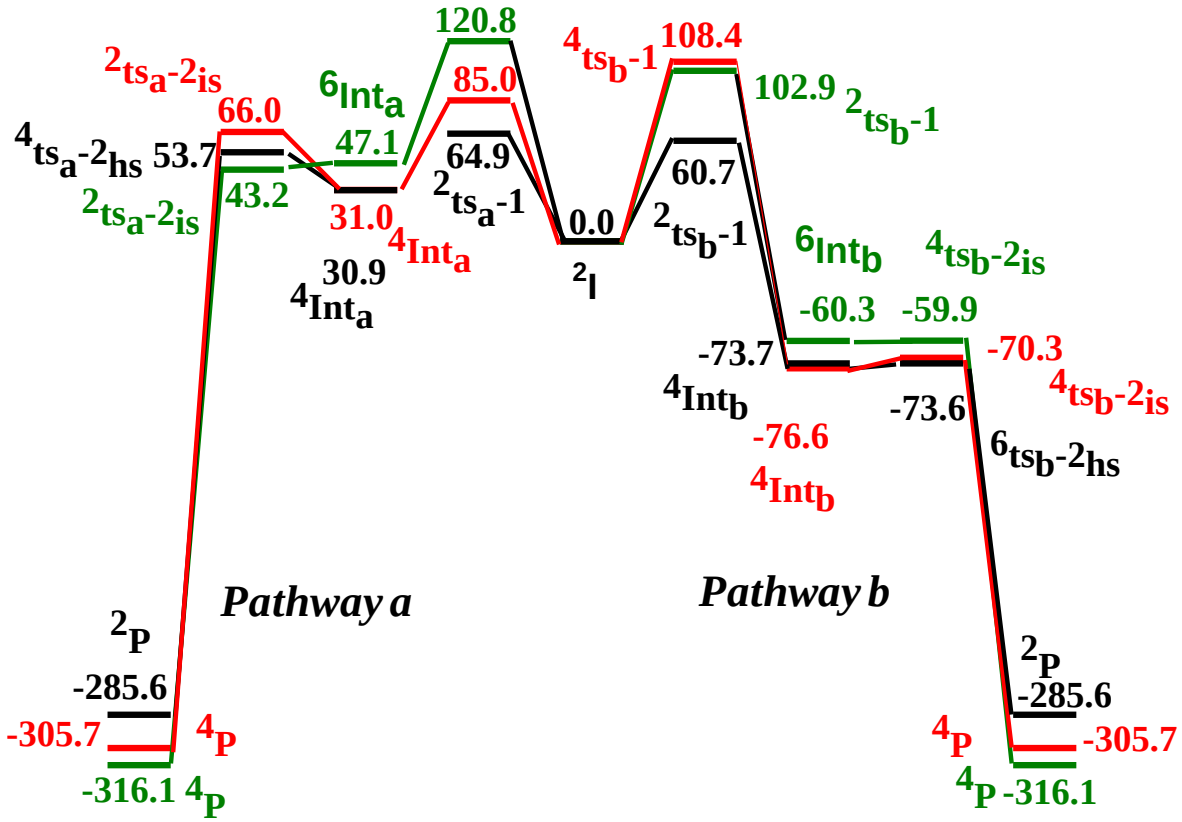

Figure 4.9. B3LYP-D2 (black), B3LYP (red) and wB97XD (olive) computed energy surface for the ground state of the ***pathway a*** and ***b*** (ΔG in $kJmol^{-1}$).

4.4. Conclusions

DFT calculations have been performed to explore the electronic structures and mechanism of formation of cyclohex-2-enone with the Fe(V)=O species. The dispersion corrected B3LYP-

D2 functional is found to perform better in predicting the correct spin states for these high valent iron-oxo species compared to B3LYP and wB97XD.[6,46]

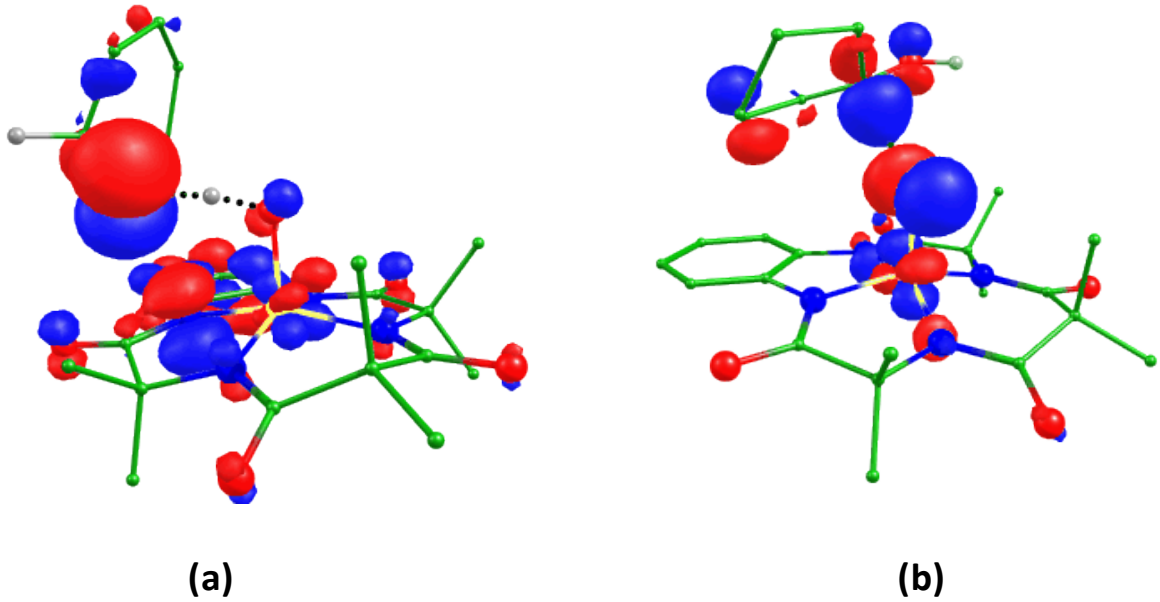

Figure 4.10. B3LYP-D2 computed HOMO of (a) $^{2}ts_{a}$-1 and (b) $^{2}ts_{b}$-1.

B3LYP-D2 also yields a lower energy barrier for the transition states compared to B3LYP and this implies that accurate estimation of the kinetics requires the incorporation of dispersion effects using density functional methods. We have explored the electronic structures and possible reaction pathways (***pathway a*** and ***pathway b***) in the course of the formation of cyclohex-2-enone from cyclohex-2-enol. We have also computed oxygen attacks on cyclohex-2-enol. DFT calculations have been used to investigate the kinetic aspects of the C-H bond activation reactions of monomeric Fe(V)-oxo unit with the tetradentate ligand. The initial H-abstraction on the low spin surface is found to be the rate-determining step for both ***pathway a*** and ***pathway b***. The computed energetic suggests that the O-H bond activation show two-state reactivity but this may not be possible in the C-H bond activation. Our calculations also predicted that the O-H/C-H bond undergoes homolytic cleavage, and it is confirmed by the significant spin density on the carbon and oxygen atoms. From the computed PES of O-H and C-H bond activation, it is apparent that the C-H bond

activation is relatively favored over the O-H bond activation which is also well supported by our computed structural parameters. Our DFT study also shows that the bond angle of the ground state of the transition state may control the reactivity. In ***pathway a***, after the O-H activation and intermediate formation, the activation of the C-H bond (second transition step) takes place which needs the barrier height of 22.8 kJ/mol, while in the ***pathway b***, after the C-H activation and formation of intermediate, there should be the O-H activation (second transition step) but it is barrier less step, and it is directly converted into the product, and formation of the product is thermodynamically favorable.

To this end, our DFT study has been employed to discuss electronic structures of a potential iron(V) oxidant and probe the mechanistic study towards allylic oxidation via C-H *vs*. O-H bond activation. This is the first computational study to discuss a comparative study on C-H *vs*. O-H bond activation along with oxygen attack towards cyclohex-2-enol by Fe(V)-oxo species. A significant exchange of metal electrons and change in structural parameters during transition states can influence reactivity and help to design a potential oxidant for catalytic transformation reactions.

4.5. References

(1) Horn, E. J.; Rosen, B. R.; Chen, Y.; Tang, J.; Chen, K.; Eastgate M. D.; Baran, P. S. *Nature* **2016**, *533*, 77-81.

(2) Nakamura, A.; Nakada, M. *Synthesis* **2013**, *45*, 1421-1451.

(3) Garcia-Cabeza, A. L.; Moreno-Dorado, F. J.; Ortega, M. J.; Guerra, F. M. *Synthesis* **2016**, *48*, 2323-2342.

(4) White, M. C. *Synlett* **2012**, *23*, 2746-2748.

(5) Groves, J. T. J. *Inorg. Biochem.* **2006**, *100*, 434-447.

(6) Ansari, A.; Kaushik, A.; Rajaraman, G. *J. Am. Chem. Soc.* **2013**, *135*, 4235-4249.

(7) Ansari, A.; Jayapal, P.; Rajaraman, G. *Angew. Chem., Int. Ed.* **2015**, *127*, 564-568.

(8) Ansari, A.; Ansari, M.; Singha, A.; Rajaraman, G. *Chem. -Eur. J.* **2017**, *23*, 10110-10125.

(9) Cavani, F.; Teles, J. H. *Chem. Sus. Chem.* **2009**, *2*, 508-534.

(10) Osterberg, P. M.; Niemeier, J. K.; Welch, C. J. ;Hawkins, J. M.; Martinelli, J. R.; Johnson, T. E.; Root, T. W.; Stahl, S. S. *Org. Process Res. Dev.* **2015**, *19*, 1537-1543.

(11) Backvall, J.-E.; Modern Oxidation Methods, Wiley-VCH Verlag GmbH, Weinheim, **2004**.

(12) Solomon, E. I.; Wong, S. D.; Liu, L. V.; Decker A.; Chow, M. S. *Curr. Opin. Chem. Biol.* **2009**, *13*, 99-113.

(13) Abu-Omar, M. M.; Loaiza, A.; Hontzeas, N. *Chem. Rev.* **2005**, *105*, 2227-2252.

(14) Solomon, E. I.; Neidig, M. L. *Chem. Commun.* **2005**, *47*, 5843-5863.

(15) Cao, Y.; Yu, H.; Peng, F.; Wang, H. *ACS Catal*. **2014**, *4*, 1617-1625.

(16) Kojima, T.; Nakayama, K.; Sakaguchi, M.; Ogura, T.; Ohkubo, K.; Fukuzumi, S. *J. Am. Chem. Soc.* **2011**, *133*, 17901-17911.

(17) Hirai, Y.; Kojima, T.; Mizutani, Y.; Shiota, Y.; Yoshizawa, K.; Fukuzumi, S. *Angew. Chem., Int. Ed.* **2008**, *47*, 5772-5776.

(18) Kojima, T.; Matsuda, Y. *Chem. Lett.* **1999**, *28*, 81-82.

(19) Que, L., Jr.; Ho Raymond, Y. N. *Chem. Rev.* **1996**, *96*, 2607-2624.

(20) Ohzu, S.; Ishizuka, T.; Hirai, Y.; Jiang, H.; Sakaguchi, M.; Ogura, T.; Fukuzumi, S.; Kojima, T. *Chem. Sci.* **2012**, *3*, 3421-3431.

(21) Qi, Y.; Luan, Y.; Yu, J.; Peng, X.; Wang, G. *Chem. -Eur. J.* **2015**, *21*, 1589-1597.

(22) Wang, J.; Yang, M.; Dong, W.; Jin, Z.; Tang, J.; Fan, S.; Lu, Y.; Wang, G. *Catal. Sci. Technol.* **2016**, *6*, 161-168.

(23) Mitra, M.; Nimir, H.; Demeshko, S.; Bhat, S. S.; Malinkin, S. O.; Haukka, M.; Lloret-Fillol, J.; Lisensky, G. C.; Meyer, F.; Shteinman, A. A. *Inorg. Chem.* **2015**, *54*, 7152-7164.

(24) Chanda, A.; Popescu, D.-L.; de Oliveira, F. T.; Bominaar, E. L.; Ryabov, A. D.; Munck, E.; Collins, T. J. *J. Inorg. Biochem*. **2006**, *100*, 606-619.

(25) Meyer, S.; Klawitter, I.; Demeshko, S.; Bill, E.; Meyer, F. *Angew. Chem., Int. Ed.* **2013**, *52*, 901-905.

(26) Rana, S.; Biswas, J. P.; Sen, A.; Clémancey, M.; Blondin, G.; Latour, J.-M.; Rajaraman, G.; Maiti, D. *Chem. Sci*. **2018**, *9*, 7843-7858.

(27) Ansari, M.; Vyas, N.; Ansari, A.; Rajaraman, G. *Dalton Trans.* **2015**, *44*, 15232-15243.

(28) Jaccob, M.; Ansari, A.; Pandey, B.; Rajaraman, G. *Dalton Trans.* **2013**, *42*, 16518-16526.

(29) Kumar, R.; Ansari, A.; Rajaraman, G. *Chem. -Eur. J.* **2018**, *24*, 6660-6860.

(30) Pandey, B.; Jaccob, M.; Rajaraman, G. *Chem. Commun*. **2017**, *53*, 3193-3196.

(31) Rohde, J.-U.; In, J.-H.; Lim, M. H.; Brennessel, W. W.; Bukowski, M. R.; Stubna, A.; Munck, E.; Nam, W.; Que, L., Jr. *Science* **2003**, *299*, 1037-1039.

(32) Nam, W. *Acc. Chem. Res*. **2007**, *40*, 522-531.

(33) Comba, P.; Rajaraman, G. *Inorg. Chem*. **2007**, *47*, 78-93.

(34) Solomon, E. I.; Brunold, T. C.; Davis, M. I.; Kemsley, J. N.; Lee, S. K.; Lehnert, N.; Neese, F.; Skulan, A. J.; Yang, Y. S.; Zhou, J. *Chem. Rev*. **2000**, *100*, 235-349.

(35) Decker, A.; Solomon, E. I. *Angew. Chem., Int. Ed.* **2005**, *44*, 2252-2255.

(36) Neese, F. *J. Inorg. Biochem*. **2006**, *100*, 716-726.

(37) Ghosh, A.; Tangen, E.; Ryeng, H.; Taylor, P. R. *Inorg. Chem*. **2004**, *2004*, 4555-4560.

(38) Kumar, D.; Hirao, H.; Que, L., Jr.; Shaik, S. *J. Am. Chem. Soc.* **2005**, *127*, 8026-8027.

(39) Kamachi, T.; Kouno, T.; Nam, W.; Yoshizawa, K. *J. Inorg. Biochem.* **2006**, *100*, 751-754.

(40) de Visser, S. P. *Angew. Chem., Int. Ed*. **2006**, *45*, 1790-1793.

(41) Pestovsky, O.; Stoian, S.; Bominaar, E. L.; Shan, X.; Münck, E.; Que, L., Jr.; Bakac, A. *Angew. Chem., Int. Ed*. **2005**, *117*, 6871-6874.

(42) Anastasi, A. E.; Comba, P.; McGrady, J.; Lienke, A.; Rohwer, H. *Inorg. Chem*. **2007**, *46*, 6420-6426.

(43) Dey, A.; Ghosh, A. *J. Am. Chem. Soc*. **2002**, *124*, 3206-3207.

(44) Filatov, M.; Harris, N.; Shaik, S. *Angew. Chem., Int. Ed.* **1999**, *38*, 3510-3512.

(45) Siegbahn, P. E. M. *Inorg. Chem.* **1999**, *38*, 2880-2889.

(46) Ansari, A.; Rajaraman, G. *Phys. Chem. Chem. Phys.* **2014**, *16*, 14601-14613.

(47) Pattanayak, S.; Jasniewski, J. A.; Rana, A.; Draksharapu, A.; Singh, K. K.; Weitz, A.; Hendrich, M.; Que, L., Jr.; Dey, A.; Gupta, S. S. *Inorg. Chem.* **2017**, *56*, 6352-6361.

(48) Sankaralingam, M.; Lee, Y.-M.; Lu, X.; Vardhaman, A. K.; Nam, W.; Fukuzumi, S. *Chem. Commun.* **2017**, *53*, 8348-8351.

(49) Kim, S. O.; Sastri, C. V.; Seo, M. S.; Kim, J.; Nam, W. *J. Am. Chem. Soc.* **2005**, *127*, 4178-4179.

(50) Groves, J. T.; Quinn, R. *J. Am. Chem. Soc.* **1985**, *107*, 5790-5792.

(51) Hong, S.; Lee, Y.-M.; Shin, W.; Fukuzumi, S.; Nam, W. *J. Am. Chem. Soc.* **2009**, *131*, 13910-13911.

(52) Lee, Y.-M.; Hong, S.; Morimoto, Y.; Shin, W.; Fukuzumi, S.; Nam, W. *J. Am. Chem. Soc.* **2010**, *132*, 10668-10670.

(53) Thibon, A. J.; Martinho, M.; Young, V. G.; Frisch, J. R., Jr.; Guillot, R. J.; Girerd, J.-J.; Munck, E.; Que, L., Jr.; Banse, F. *Angew. Chem., Int. Ed*. **2008**, *47*, 7064-7067.

(54) Hong, S.; Lee, Y.-M.; Sankaralingam, M.; Vardhaman, A. K.; Park, Y. J.; Cho, K.-B.; Ogura, T.; Sarangi, R.; Fukuzumi, S.; Nam, W. *J. Am. Chem. Soc.* **2016**, *138*, 8523-8532.

(55) Nishida, Y.; Lee, Y.-M.; Nam, W.; Fukuzumi, S. *J. Am. Chem. Soc.* **2014**, *136*, 8042-8049.

(56) Li, F.; Van Heuvelen, K. M.; Meier, K. K.; Munck, E.; Que, L., Jr. *J. Am. Chem. Soc.* **2013**, *135*, 10198-10201.

(57) Comba, P.; Lee, Y.-M.; Nam, W.; Waleska, A. *Chem. Commun.* **2014**, *50*, 412-414.

(58) Mahammed, A.; Gray, H. B.; Meier-Callahan, A. E.; Gross, Z. *J. Am. Chem. Soc.* **2003**, *125*, 1162-1163.

(59) Liu, S.; Mase, K.; Bougher, C.; Hicks, S. D.; Abu-Omar, M. M.; Fukuzumi, S. *Inorg. Chem.* **2014**, *53*, 7780-7788.

(60) Mills, M. R.; Burton, A. E.; Mori, D. I.; Ryabov, A. D.; Collins, T. J. *J. Coord. Chem.* **2015**, *68*, 3046-3057.

(61) Price, J. C.; Barr, E. W.; Glass, T. E.; Krebs, C.; Bollinger, J. M. *J. Am. Chem. Soc.* **2003**, *125*, 13008-13009.

(62) Price, J. C.; Barr, E. W.; Tirupati, B.; Bollinger, J. M.; Krebs, C. *Biochemistry* **2003**, *42*, 7497-7508.

(63) de Oliveira, F. T.; Chanda, A.; Banerjee, D.; Shan, X.; Mondal, S.; Que, L., Jr.; Bominaar, E. L.; Munck, E.; Collins, T. J. *Science* **2007**, *315*, 835-838.

(64) Lyakin, O. Y.; Bryliakov, K. P.; Britovsek, G. J. P.; Talsi, E. P. *J. Am. Chem. Soc.* **2009**, *131*, 10798-10799.

(65) Prat, I.; Mathieson, J. S.; Guell, M.; Ribas, X.; Luis, J. M.; Cronin, L.; Costas, M. *Nat. Chem.* **2011**, *3*, 788-793.

(66) McDonald, A. R.; Que, L., Jr. *Nat. Chem.* **2011**, *3*, 761-762.

(67) Van Heuvelen, K. M.; Fiedler,A. T.; Shana, X.; De Hont, R. F.; Meier, K. K.; Bominaar, E. L.; Munck, E.; Que, L., Jr. *Proc. Natl. Acad. Sci. U.S.A.*, **2012**, *109*, 11933-11938.

(68) Makhlynets, O. V.; Rybak-Akimova, E. V. *Chem. -Eur. J.* **2010**, *16*, 13995-14006.

(69) Que, L., Jr.; Tolman, W. B. *Nature* **2008**, *455*, 333-340.

(70) Ho, R. Y. N.; Roelfes, G.; Feringa, B. L.; Que, L., Jr. *J. Am. Chem. Soc.* **1999**, *121*, 264-265.

(71) Weiss, R.; Bulach, V.; Gold, A.; Terner, J.; Trautwein, A. X. *J. Biol. Inorg. Chem.* **2001**, *6*, 831-845.

(72) Comba, P.; Maurer, M.; Vadivelu, P. *J. Phys. Chem. A* **2008**, *112*, 13028-13036.

(73) Quinonero, D.; Morokuma, K.; Musaev, D. G. *J. Am. Chem. Soc.* **2005**, 127, 6548-6549.

(74) Chakrabarty, S.; Austin, R. N.; Deng, D.; Groves, J. T.; Lipscomb, J. D. *J. Am. Chem. Soc.* **2007**, *129*, 3514-3515.

(75) Bassan, A.; Blomberg, M. R.; Siegbahn, A. P. E. M.; Que, L., Jr. *Chem. -Eur. J.* **2005**, *11*, 692-705.

(76) Comba, P.; Maurer, M.; Vadivelu, P. *J. Phys. Chem.* A **2008**, *112*, 13028-13036.

(77) Costas, M.; Mehn, M. P.; Jensen, M. P.; Que, L., Jr. *Chem. Rev*. **2004**, *104,* 939-986.

(78) Klinker, E. J.; Kaizer, J.; Brennessel, W. W.; Woodrum, N. L.; Cramer, C. J.; Que, L., Jr. *Angew. Chem., Int. Ed.* **2005**, *44*, 3690-3694.

(79) Decker, A.; Rohde, J.-U.; Que, L., Jr.; Solomon, E. I. *J. Am. Chem. Soc.* **2004**, *126*, 5378-5379.

(80) Jensen, M. P.; Lange, S. J.; Mehn, M. P.; Que, E. L.; Que, L., Jr. *J. Am. Chem. Soc.* **2003**, *125*, 2113-2128.

(81) Aquino, F.; Rodriguez, J. H. *J. Chem. Phys.* **2005**, *123*, 204902-204906.

(82) Chow, T. W.-S.; Wong, E. L.-M.; Guo, Z.; Liu, Y.; Huang, J.-S.; Che, C.-M. *J. Am. Chem. Soc.* **2010**, *132*, 13229-13239.

(83) Sankaralingam, M.; Lee, Y.-M.; Nam, W.; Fukuzumi, S. *Inorg. Chem.* **2017**, *56*, 5096-5104.

(84) Punniyamurthy, T.; Rout, L. *Coord. Chem. Rev*. **2008**, *252*, 134-154.

(85) Dapurkar, S. E.; Kawanami, H.; Komura, K.; Yokoyama, T.; Ikushima, Y. *Appl. Catal.* **2008**, *346*, 112-116.

(86) Salavati-Niasari, M. M.; Elzami, R.; Mansournia, M. R.; Hydarzadeh, S. *J. Mol. Catal. A: Chem.* **2004**, *221*, 169-175.

(87) Mukherjee, S.; Samanta, S.; Roy, B. C.; Bhaumik, A. *Appl. Catal. A* **2006**, *301*, 79-88.

(88) Jiang, D.; Mallat, T.; Meier, D. M.; Urakawa, A.; Baiker, A. *J. Catal.* **2010**, *270*, 26-33.

(89) Wang, R. M.; Duan, Z. F.; He, Y. F.; Lei, Z. Q. *J. Mol. Catal. A: Chem*. **2006**, *260*, 280-287.

(90) Newhouse, T.; Baran, P. S. *Angew. Chem., Int. Ed.* **2011**, *50*, 3362-3374.

(91) Fraunhoffer, K. J.; Prabagaran, N.; SiroisL, E.; White, M. C. *J. Am. Chem. Soc*. **2006**, *128,* 9032-9033.

(92) Covell, D. J.; Vermeulen, N. A.; Labenz, N. A.; White, M. C. *Angew. Chem., Int. Ed.* **2006**, *118,* 8397-8400.

(93) Ginotra S. K.; Singh, V. K. *Org. Biomol. Chem*. **2006**, *4*, 4370-4374.

(94) Fraunhoffer, K. J.; Bachovchin, D. A.; White, M. C. *Org. Lett*. **2005**, *7,* 223-226.

(95) Zhou, J.; Tang, Y. *Chem. Soc. Rev.* **2005**, *34*, 664-676.

(96) Andrus, M. B.; Asgari, D. *Tetrahedron* **2000**, *56*, 5775-5780.

(97) Kwon, Y. H.; Mai, B. K.; Lee, Y.-M.; Dhuri, S. N.; Mandal, D.; Cho, K.-B.; Kim, Y.; Shaik, S.; Nam, W. *J. Phys. Chem. Lett.* **2015**, *6*, 1472-1476.

(98) Dhuri, S. N.; Cho, K.-B.; Lee, Y.-M.; Shin, S. Y.; Kim, J. H.; Mandal, D.; Shaik, S.; Nam, W. *J. Am. Chem. Soc.* **2015**, *137*, 8623-8632.

(99) Mandal, D.; Ramanan, R.; Usharani, D.; Janardanan, D.; Wang, B.; Shaik, S. *J. Am. Chem. Soc.* **2015**, *137*, 722-733.

(100) Dakdouki, S. C.; Villemin, D.; Bar, N. *Eur. J. Org. Chem.* **2011**, *2011*, 4448-4454.

(101) Cusso, O.; Cianfanelli, M.; Ribas, X.; Gebbink, R. J. M. K.; Costas, M. *J. Am. Chem. Soc.* **2016**, *138*, 2732-2738.

(102) Li, J. S.; Qiu, Z.; Li, C. J. *Adv. Synth. Catal.* **2017**, *359*, 3648-3653.

(103) Ghosh, M.; Nikhil, Y. L. K.; Dhar, B. B.; Sen Gupta, S. *Inorg. chem.* **2015**, *54*, 11792-11798.

(104) Wang, Z. B.; Zhang, Q.; Lu, X. F.; Chen S. J.; Liu, C. J. *Chin. J. Catal.* **2015**, *36*, 400-407.

(105) Zhou, G. B.; Dou, R. F.; Bi, H. Z.; Xie, S. H.; Pei, Y.; Fan, K. N. M.; Qiao, H.; Sun, B.; Zong, B. N. *J. Catal.* **2015**, *332*, 119-126.

(106) Sun, H. J.; Pan, Y. J.; Li, S. H.; Zhang, Y. X.; Dong, Y. Y.; Liu, S. C.; Liu, Z. Y. *J. Energy. Chem.* **2013**, *22*, 710-716.

(107) Li, Z. L.; Lv, A.; Li, L.; Deng, X. X.; Zhang, L. J.; Du, F. S.; Li, Z. C. *Polymer* **2013**, *54*, 3841-3849

(108) Dakdouki, S. C.; Villemin, D.; Bar, N. *Eur. J. Org. Chem.* **2011**, *23*, 4448-4454.

(109) Frisch, M. J.; Trucks, G. W.; Schlegel, H. B.; Scuseria, G. E.; Robb, M. A.; Cheeseman, J. R.; Scalmani, G.; Barone, V.; Petersson, G. A.; Nakatsuji, H.; Li, X.; Caricato, M.; Marenich, A. V.; Bloino, J.; Janesko, B. G.; Gomperts, R.; Mennucci, B.; Hratchian, H. P.; Ortiz, J. V.; Izmaylov, A. F.; Sonnenberg, J. L.; Williams-Young, D.; Ding, F.; Lipparini, F.; Egidi, F.; Goings, J.; Peng, B.; Petrone, A.; Henderson, T.; Ranasinghe, D.; Zakrzewski, V. G.; Gao, J.; Rega, N.; Zheng, G.; Liang, W.; Hada, M.; Ehara, M.; Toyota, K.; Fukuda, R.; Hasegawa, J.; Ishida, M.; Nakajima, T.; Honda, Y.; Kitao, O.; Nakai, H.; Vreven, T.; Throssell, K.; Montgomery, J. A., Jr.; Peralta, J. E.; Ogliaro, F.; Bearpark, M. J.; Heyd, J. J.; Brothers, E. N.; Kudin, K. N.; Staroverov, V. N.; Keith, T. A.; Kobayashi, R.; Normand, J.; Raghavachari, K. A.; Rendell, P.; Burant, J. C.; Iyengar, S. S.; Tomasi, J.; Martin, C. M.; Millam, J. M.; Klene, M.; Adamo, C.; Cammi, R.; Ochterski, J. W.; Morokuma, R. L. K. O.; Farkas, F. J. B.; Fox, D. J. Gaussian, Inc., Wallingford CT, 2016.

(110) Becke, A. D. *J. Chem. Phys*. **1993**, *98*, 5648-5652.

(111) Lee, C.; Yang, W.; Parr, R. G. *Phys. Rev. B: Condens. Matter Mater. Phys*. **1988**, *37*, 785-789.

(112) Grimme, S. *J. Comput. Chem.* **2006**, *27*, 1787-1799.

(113) Chai, J. D.; Head-Gordon, M. *Phys. Chem. Chem. Phys.* **2008**, *10*, 6615-6620.

(114) Tao, J. M.; Perdew, J. P.; Staroverov, V. N.; Scuseria, G. E. *Phys. Rev. Lett.* **2003**, *91*, 146401-146404.

(115) Handy, N. C.; Cohen, A. *J. Mol. Phys.* **2001**, *99*, 401-413.

(116) Møller, C.; Plesset, M. S. *Phys. Rev.* **1934**, *46*, 618-622.

(117) Zhao, Y.; Truhlar, D. G. *Theor. Chem. Acc.* **2008**, *120*, 215-241.

(118) Grimme, S. *J. Comput. Chem.* **2006**, *27*, 1787-1799.

(119) Becke, A. D. *J. Chem. Phys*. **1993**, *98*, 5648-5652.

(120) Lee, C.; Yang, W.; Parr, R. G. *Phys. Rev. B: Condens. Matter Mater. Phys*. **1988**, *37*, 785-789.

(121) Kepp, K. P. *J. Inorg. Biochem*. ***2011***, *105*, 1286-1292.

(122) Hirao, H.; Kumar, D.; Que, L., Jr.; Shaik, S. *J. Am. Chem. Soc.* **2006**, *128*, 8590-8606.

(123) Hiro, H.; Kumar, D.; Thiel, W.; Shaik, S. *J. Am. Chem. Soc.* **2005**, *127*, 13007-13018.

(124) Bathelt, C. M.; Zurek, J.; Mulholland, A. J.; Harvey, J. N. *J. Am. Chem. Soc.* **2005**, *127*, 12900-12908.

(125) Bassan, A.; Blomberg, M. R. A.; Siegbahn, P. E. M.; Que, L., Jr. *Angew. Chem., Int. Ed.* **2005**, *44*, 2939-2941.

(126) Siegbahn, P. E. M. *J. Biol. Inorg. Chem*. **2006**, *11*, 695-701.

(127) Siegbahn, P. E. M.; Borowski, T. *Acc. Chem. Res*. **2006**, *39*, 729-738.

(128) Ghosh, A. *J. Biol. Inorg. Chem*. **2006**, *11*, 671-673.

(129) Ghosh, A. *J. Biol. Inorg. Chem*. **2006**, *11*, 712-724.

(130) Neese, F. *J. Biol. Inorg. Chem.* **2006**, *11*, 702-711.

(131) Noodleman, L. W.; Han, G. *J. Biol. Inorg. Chem*. **2006**, *11*, 674-694.

(132) Olsson, E.; Martinez, A.; Teigen, K.; Jensen, V. R. *Chem. -Eur. J.* **2011**, *17*, 3746-3758.

(133) Olsson, E.; Mertinez, A.; Teigen, K.; Jensen, V. R. *Inorg. Chem.* **2011**, *17*, 2720-2732.

(134) Dunning, T. H., Jr.; Hay, P. J. *In Modern Theoretical Chemistry* (Ed: Schaefer, H. F.), Plenum, New York, **1976**; Vol. 3.

(135) Hay, P. J.; Wadt, W. R. *J. Chem. Phys.* **1985**, 82, 270-283.

(136) Hay, P. J.; Wadt, W. R. *J. Chem. Phys.* **1985**, *82,* 299-310.

(137) Wadt, W. R.; Hay, P. J. *J. Chem. Phys.* **1985**, *82,* 284-298.

(138) Schaefer, A.; Horn, H.; Ahlrichs, R. *J. Chem. Phys.* **1992**, *97*, 2571-2577.

(139) Schaefer, C.; Huber, C. ;Ahlrichs, R. *Chem. Phys.* **1994**, *100*, 5829-5835.

(140) Zhurko, G. A. *Chemcraft software, version 1.6*, **2014**.

(141) Dunn, P. J.; Hii, K. K.; Krische, M. J.; Williams, M. T. Sustainable Catalysis: Challenges and Practices for the Pharmaceutical and Fine Chemical Industries, John Wiley & Sons, Inc, 1st Ed., Weinheim, **2013**, pp. 121-137

(142) Kaloglu, M.; Gürbüz, N.; Semeril, D.; Ozdemir, I. *Inorg. Chem.* **2018**, *10*, 1236-1243.

(143) Warren, J. J.; Tronic, T. A.; Mayer, J. M. *Chem. Rev.* **2010**, *110*, 6961-7001.

(144) Fiedler, T.; Que, L., Jr. *Inorg. Chem.* **2009**, *48,* 11038-11047.

(145) Cho, K.-B.; Wu, X.; Lee, Y.-M.; Kwon, Y. H.; Shaik, S.; Nam, W. *J. Am. Chem. Soc.* **2012**, *134*, 20222-20225**.**

(146) Gaggioli, C. A.; Sauer, J.; Gagliardi, L. *J. Am. Chem. Soc.* **2019**, *141*, 14603-14611.

(147) Mondal, B.; Neese, F.; Bill, E.; Ye, S. *J. Am. Chem. Soc.* **2018**, *140*, 9531-9544.

(148) Mukherjee, G.; Lee, C. W. Z.; Nag, S. S.; Alili, A.; Reinhard, F. G. C.; Kumar, D.; Sastri, C. V.; de Visser, S. P. *Dalton Trans.* **2018**, *47*, 14945-14957.